



Meridional circulation during the Last Glacial Maximum explored through a combination of South Atlantic $\delta^{18}\text{O}$ observations and a geostrophic inverse model

Geoffrey Gebbie

Department of Earth and Planetary Sciences, Harvard University, 24 Oxford Street, Cambridge, Massachusetts 02138, USA (gebbie@eps.harvard.edu)

Peter Huybers

Department of Earth and Planetary Sciences, Harvard University, 24 Oxford Street, Cambridge, Massachusetts 02138, USA

Woods Hole Oceanographic Institution, Woods Hole, Massachusetts, USA

[1] The vertical profile of meridional transport in the South Atlantic is examined by combining paleoceanographic observations with a geostrophic circulation model using an inverse method. $\delta^{18}\text{O}_{\text{calcite}}$ observations along the margins of the South Atlantic show that upper-ocean cross-basin differences were weaker during the Last Glacial Maximum (LGM) than the Holocene. The $\delta^{18}\text{O}_{\text{calcite}}$ observations can be explained by a shift of water-mass properties without any change in the overturning circulation. Alternatively, they may indicate a reduced LGM cross-basin density difference and, via the thermal wind relation, a reduced vertical shear. Model inversions of $\delta^{18}\text{O}_{\text{calcite}}$ are found to require meridional transports different from the modern only after three assumptions are made: temperature and salinity distributions are spatially smooth, the relationship between salinity and $\delta^{18}\text{O}_{\text{water}}$ is linear and spatially invariant, and LGM temperatures are known to within 1°C along the margins. The last assumption is necessary because an independent constraint on temperature or salinity is required to determine density from $\delta^{18}\text{O}_{\text{calcite}}$ observations. $\delta^{18}\text{O}_{\text{calcite}}$ observations are clearly useful, but before any firm constraints can be placed on LGM meridional transport, it appears necessary to better determine the relationship between $\delta^{18}\text{O}_{\text{calcite}}$ and density.

Components: 8223 words, 9 figures.

Keywords: inverse modeling; Last Glacial Maximum; meridional ocean circulation; geostrophy.

Index Terms: 3260 Mathematical Geophysics: Inverse theory; 4924 Paleoceanography: Geochemical tracers.

Received 6 June 2006; **Revised** 16 August 2006; **Accepted** 18 September 2006; **Published** 15 November 2006.

Gebbie, G., and P. Huybers (2006), Meridional circulation during the Last Glacial Maximum explored through a combination of South Atlantic $\delta^{18}\text{O}$ observations and a geostrophic inverse model, *Geochem. Geophys. Geosyst.*, 7, Q11N07, doi:10.1029/2006GC001383.

Theme: Past Ocean Circulation

Guest Editors: Jean Lynch-Stieglitz, Catherine Kissel, and Olivier Marchal

1. Introduction

[2] Given the large climatic shifts between the Last Glacial Maximum (LGM) and Holocene evident in, for example, sea level [e.g., *Thompson and Goldstein*, 2005], sea surface temperatures [e.g., *Kucera et al.*, 2006], and ocean nutrients [e.g., *Curry and Oppo*, 2005], one expects ocean circulation to have changed. But to determine how the mass circulation changed (and not only that it was different) requires distinguishing between a multitude of plausible scenarios, a demanding task for the available paleoceanographic proxies. Most studies of past ocean circulation depend either on models or observations, and look to the other for tests of consistency. Here we attempt to more explicitly combine these approaches. In particular, we seek to combine observations of $\delta^{18}\text{O}_{\text{calcite}}$ taken along the margins of the South Atlantic, presented in this theme by [*Lynch-Stieglitz et al.*, 2006], with a model of ocean transport using inverse methods [e.g., *Wunsch*, 1996]. Our goal is to test whether the LGM $\delta^{18}\text{O}_{\text{calcite}}$ observations demand a meridional circulation different from the modern, and if so, to estimate how it was different.

[3] Previous attempts to constrain past ocean circulation using inverse methods have demonstrated the problem to be a challenging one [*Legrand and Wunsch*, 1995; *Winguth et al.*, 2000; *Huybers et al.*, 2006]. *Legrand and Wunsch* [1995] attempted to determine whether the southward flow of North Atlantic Deep Water (NADW) had changed during the LGM using $\delta^{13}\text{C}$ observations. They were unable to constrain rates of flow, consistent with the interpretation of $\delta^{13}\text{C}$ being primarily a passive tracer of the ocean circulation [*Boyle*, 1990]. Another study which addressed the LGM Atlantic circulation was conducted by *Winguth et al.* [2000] in which an ocean general circulation model was brought into consistency with Cd/Ca and $\delta^{13}\text{C}$ distributions through adjustments made to the surface salinity values. In this case, the model achieved a better fit with the data when meridional transport was reduced and deep water originating from the northern North Atlantic was more shallow. But whether other changes, such as circulations with different rates of flow, could also explain the data is unknown.

[4] Over the last decade, important new proxies have been developed which have the potential to better constrain dynamical features of the past ocean circulation, including radiocarbon [e.g., *Robinson et al.*, 2005], Pa/Th ratios [e.g., *McManus et al.*, 2004],

and the use of $\delta^{18}\text{O}_{\text{calcite}}$ as a proxy for density [e.g., *Lynch-Stieglitz et al.*, 1999]. In an extension of the study by *Legrand and Wunsch* [1995], *Huybers et al.* [2006] explored the ability of $\delta^{18}\text{O}_{\text{calcite}}$ and $\Delta^{14}\text{C}$ to constrain meridional transport in an idealized basin. In particular, they sought to determine which proxy observations are required to constrain rates of meridional transport, given that any three-dimensional flow consistent with dynamical constraints is permissible. It was found that uncertainties in presently available proxy measurements are an order of magnitude too large to bound rates of meridional circulation within a factor of two.

[5] Here we ask a more specific question than that of *Huybers et al.* [2006], whether observations of LGM $\delta^{18}\text{O}_{\text{calcite}}$ require a vertical structure of meridional mass transport different from the modern circulation. The question of this study is more stringent and will hopefully allow distinctions to be made between the modern and glacial circulations. Section 2 describes the relationship between $\delta^{18}\text{O}_{\text{calcite}}$ and the density of seawater, section 3 introduces a geostrophic model and briefly reviews the inverse method which is applied, section 4 gives results from various inversions of the data, and conclusions are made in section 5.

2. Interpreting $\delta^{18}\text{O}$

[6] This study is motivated by the availability of a new cross-Atlantic $\delta^{18}\text{O}_{\text{calcite}}$ data set measured and assembled by *Lynch-Stieglitz et al.* [2006]. Observations span depths on both sides of the Atlantic from 200 to 2000 meters. To the west, benthic foraminiferal $\delta^{18}\text{O}_{\text{calcite}}$ observations all come from within a few degrees of 27°S, near the margin of southern Brazil. To the east, observations were taken along the African margin from as far north as 4°S and south to 34°S. The location of each observation is indicated in Figure 1. For simplicity, and in keeping with the approach of *Lynch-Stieglitz et al.* [2006], we analyze the data in terms of a zonal cross-section at 30°S. Along the African margin at 300 meters depth, temperature varies by up to 3°C and salinity by 0.5 in the modern climatology, so the error introduced by using a zonal section is not negligible and will be taken up again later in this work.

[7] $\delta^{18}\text{O}_{\text{calcite}}$ depends upon both the $\delta^{18}\text{O}$ and temperature of the seawater in which precipitation occurs: $\delta^{18}\text{O}_{\text{calcite}} = f(\delta^{18}\text{O}_{\text{water}}, T)$. An approximately linear relationship exists between $\delta^{18}\text{O}_{\text{calcite}}$ and temperature, and the above equation

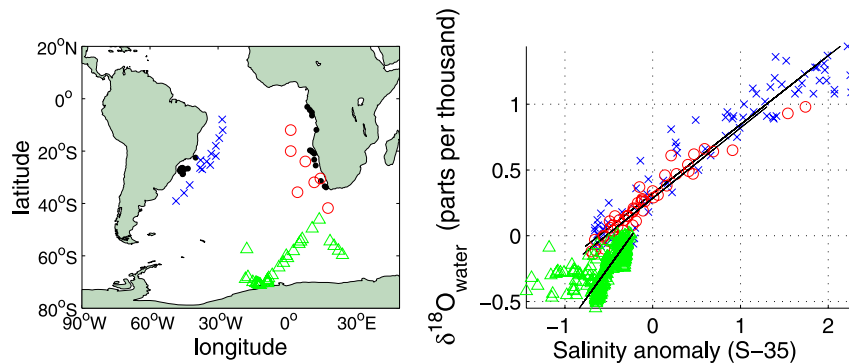


Figure 1. (left) Map indicating the location of the proxy data sites (black dots) from which $\delta^{18}\text{O}_{\text{calcite}}$ was sampled and modern hydrographic sites (crosses, circles, and triangles) where $\delta^{18}\text{O}_{\text{water}}$ and salinity observations are available. (right) Modern salinity and $\delta^{18}\text{O}_{\text{water}}$ observations [from Schmidt *et al.*, 1999] with least squares best fits for the Brazil (crosses), African (circles), and Southern Ocean (triangles) regions.

can be rewritten: $\delta^{18}\text{O}_{\text{calcite}} = \delta^{18}\text{O}_{\text{water}} + cT + d$, where the temperature-dependent slope is taken as $c = -0.22\text{‰}/^{\circ}\text{C}$ and d is a constant. Furthermore, $\delta^{18}\text{O}_{\text{water}}$ positively co-varies with salinity so that their relationship can also be modeled as a linear function: $\delta^{18}\text{O}_{\text{water}} = a S' + b$, where S' is the salinity anomaly and b is a constant. Salinity is measured according to the practical salinity scale, and the salinity anomaly is defined relative to a baseline salinity of 35. (Although salinity is therefore dimensionless, it can be interpreted in a physically meaningful and sufficiently accurate way as having units of ‰.) Putting these two independent relationships together, one can write an equation for the dependence of $\delta^{18}\text{O}_{\text{calcite}}$ on temperature and salinity:

$$\delta^{18}\text{O}_{\text{calcite}} = aS' + b + cT + d. \quad (1)$$

[8] The temperature coefficient, c in (1), is well-determined by the chemistry of calcification. The salinity coefficient a is less well constrained and is estimated here using modern observations of $\delta^{18}\text{O}_{\text{water}}$ and salinity [Schmidt *et al.*, 1999]. A least squares fit of observations in the South Atlantic above 2000 meters yields $a = 0.48 \pm 0.02\text{‰}$. In the inverse model (to be detailed in section 3), we use $a = 0.5\text{‰}$. The b and d coefficients are treated as a single, summed constant. To find the Holocene value of $b + d$, equation (1) is solved to give a least squares best fit with the modern temperature and salinity, yielding a value of 3.5‰ and a standard deviation of the residual of 0.17‰ .

[9] It is also necessary to estimate the coefficients of (1) for the LGM. In the absence of evidence to the contrary, we assume that a and c are unchanged from Holocene values for the LGM. Average values of

$\delta^{18}\text{O}_{\text{calcite}}$ were larger during the LGM, owing to the buildup of isotopically depleted oxygen in the ice sheets and a global-mean cooling. Also, the mean salinity of the ocean was slightly increased owing to storage of freshwater in ice sheets. A least squares fit of equation (1), again using modern temperature and salinity, yields $b + d = 5.2\text{‰}$ for the LGM. Note that the cross-basin difference in $\delta^{18}\text{O}_{\text{calcite}}$ plays the primary dynamical role, and therefore the later results of this work are insensitive to the spatially uniform value of $b + d$.

[10] It is useful to consider some of the limitations inherent to the assumptions made in relating $\delta^{18}\text{O}_{\text{water}}$ and salinity. Their relationship is affected by a number of processes [Rohling and Bigg, 1998]; for example, sea-ice formation leads to brine rejection but only weak fractionation of oxygen isotopes, evaporation partially fractionates oxygen but the evaporated water contains almost no salt, and the effect of precipitation on $\delta^{18}\text{O}_{\text{water}}$ involves both temperature and the past history of the water parcel. The linear $\delta^{18}\text{O}_{\text{water}}$ – salinity equation introduced above is a crude parameterization, and a coupled atmosphere-ocean model would provide a more complete representation of the $\delta^{18}\text{O}_{\text{water}}$ cycle [e.g., Schmidt, 1998].

[11] The regression coefficients between $\delta^{18}\text{O}_{\text{water}}$ and salinity are sensitive to the geographic domain over which they are calculated. For example, a has been estimated as 0.48‰ using modern $\delta^{18}\text{O}_{\text{water}}$ observations at depths between the surface and 2000 meters in the South Atlantic, but if the depth range is restricted between 200 and 2000 meters, a instead is 0.6‰ . If data from the North Atlantic are instead used, then a is 0.1‰ . The right panel of Figure 1 shows a more detailed regional comparison: $a = 0.44 \pm 0.02\text{‰}$ and $b = 0.35 \pm 0.02\text{‰}$ on

the Brazil margin, $a = 0.44 \pm 0.02\%$ and $b = 0.28 \pm 0.01\%$ on the African margin, and $a = 0.44 \pm 0.02\%$ and $b = 0 \pm 0.01\%$ south and west of Africa. The estimated slope is fairly consistent, while the intercept varies widely. The low values of $\delta^{18}\text{O}_{\text{water}}$ in the Southern Ocean are presumably related to the increased fractionation of precipitation toward higher latitudes and to calving and melting of Antarctic ice [Toggweiler and Samuels, 1995]. Mixing of water-masses originating in the Southern Ocean with those on the African margin could account for the lower values of b relative to the Brazil margin. Therefore cross-basin differences in $\delta^{18}\text{O}_{\text{calcite}}$ are potentially influenced by differences in the mean value of $\delta^{18}\text{O}_{\text{water}}$. While we have assumed that a and b have no spatial variations, this assumption does not strictly hold.

[12] Apart from spatial variations, it appears that the coefficients of (1) may have varied through time. For example, Adkins *et al.* [2002] showed that LGM bottom waters at four sites had a much higher salinity to $\delta^{18}\text{O}_{\text{water}}$ ratio than modern waters. Deep waters at the Shona Rise (south of the African margin) were the saltiest of the four sites during the LGM, but this is not the case in the modern salinity field. Modeling studies also indicate that the salinity- $\delta^{18}\text{O}_{\text{water}}$ relationship will vary with climate [Rohling and Bigg, 1998; LeGrande *et al.*, 2006].

[13] To reiterate, we make three simplifying assumptions to gain traction in the problem: changes in $\delta^{18}\text{O}_{\text{calcite}}$ reflect vertical (not meridional) variations, the slope between $\delta^{18}\text{O}_{\text{calcite}}$ and salinity is fixed at $0.5\Delta\%/\Delta S$, and that there are no spatial or temporal variations in b and d . Pending the development of further constraints on the density- $\delta^{18}\text{O}_{\text{calcite}}$ relationship, these assumptions permit exploration of the dynamical implications of the $\delta^{18}\text{O}_{\text{calcite}}$ observations.

3. Model

[14] The model domain is a two-dimensional section of the South Atlantic Ocean along 30°S. The entire vertical water column is included, and the section runs from South America to Africa. The grid has a horizontal resolution of 1° and vertical resolution of 120 meters. The model state includes two-dimensional fields of temperature, salinity, and meridional velocity. The model is a steady-state geostrophic inverse model, following Wunsch [1978] and many subsequent authors.

[15] Over long time periods and large spatial scales, the ocean circulation is observed, within good approximation, to be in both geostrophic and hydrostatic balance. Together, these two balances give the thermal wind relation:

$$\frac{\partial v}{\partial z} = -\frac{g}{f\rho_0} \frac{\partial \rho}{\partial x} + \epsilon, \quad (2)$$

in which v is the meridional geostrophic velocity, g is gravity, f is the Coriolis parameter, ρ is density, and ϵ is present because the balance is not perfect. The oceanic density field varies by only a small fraction about its mean, so ρ is approximated by a constant $\rho_0 = 1035 \text{ kg/m}^3$ outside of the derivative with only a small loss of accuracy. The thermal wind relation dictates that vertical shear is balanced primarily by horizontal density gradients.

[16] The imbalance ϵ can be due to a breakdown in hydrostatic or geostrophic balance. Scaling arguments show that errors in hydrostatic balance are $O(\delta) \approx 10^{-3}$ where δ is the aspect ratio of oceanic motions. To good approximation, therefore, errors from hydrostatic balance are negligible. The accuracy of geostrophic balance is determined by the Rossby number (i.e., $Ro = U/fL$, where U is a velocity scale, f is the Coriolis parameter, and L is a length scale). To estimate the size of ϵ , we compute the implied vertical shear from the modern density observations and assume that the ageostrophic component of the shear will be smaller by a ratio given by the Rossby number. Plausible modern estimates of the Rossby number range as high as 0.01 or 0.1 for large-scale flows. Using the intentionally small Rossby number of 0.001 gives an expected standard deviation for ϵ of $2 \times 10^{-5} \text{ s}^{-1}$. (This uncertainty translates to 0.0002 Sv for each grid face.) A small uncertainty is selected for the thermal wind relation to give observations the best chance of constraining the circulation, but this assumption would need to be revisited prior to drawing firm conclusions regarding past ocean circulation.

[17] To demonstrate the use of the thermal wind relation, consider a rectangular slice of the ocean between two depths, z_1 and z_2 , and two horizontal points, x_1 and x_2 , at the same latitude. The transport through the section is calculated by integrating (2) over the rectangle:

$$V(x_1, x_2, z_1, z_2) = -\frac{g}{f} \int_{z_2}^{z_1} (\rho(x_2, z) - \rho(x_1, z)) dz + V_o, \quad (3)$$

where V has units of m^2/s . Transport depends on the density at the sides and one unknown

integration constant, as discussed by *Marotzke et al.* [1999] and *Lynch-Stieglitz* [2001]. In the case that the slice intersects the seafloor, the transport equation is no longer valid. Note that the Rio Grande Rise and Mid-Atlantic Ridge come within 2300 and 2200 meters of the present-day surface, respectively, and the influence of the topography in the South Atlantic must be considered.

[18] The constant V_o in equation (3) arises because the thermal wind relation only constrains the vertical shear and not the depth-independent velocity, a classic issue known as the reference level problem. Additional information is required to solve for V_o . In this case the basin-wide section provides the additional constraint of conservation of mass or, nearly equivalently, conservation of volume. Total volume transport across the section at 30°S is assumed to balance the relatively small inflow from the Arctic Ocean, freshwater fluxes (evaporation, precipitation, and runoff), and changes in sea level. Observed imbalances and their uncertainties are detailed in section 4.1.

[19] The thermal wind relation and volume conservation are discretized onto the model grid already defined. Each grid box corner carries a temperature and salinity value from which density is diagnosed. The equation of state is linearized about a mean profile as a function of depth for temperature, $\bar{T}(z)$, and salinity, $\bar{S}(z)$, from the HydroBase2 climatology [Curry, 2002],

$$\rho = \alpha(z)T' + \beta(z)S' + \gamma(z), \quad (4)$$

where T' and S' are anomalies relative to the mean profile, $\alpha(z)$ is the depth-dependent thermal expansion coefficient, $\beta(z)$ is the haline contraction coefficient, and $\gamma(z)$ is an offset profile that accounts for shifts in the mean density. Equation (4) is written in a nontraditional form to make the similarity with equation (1) for $\delta^{18}\text{O}_{\text{calcite}}$ more obvious. Also note that only horizontal gradients of density appear in the thermal wind balance so that $\gamma(z)$ has no dynamical role.

[20] Any observation which can be expressed as a function of the model variables can be included in the inverse formulation. In many cases, the state variables are directly observed, such as temperature. $\delta^{18}\text{O}_{\text{calcite}}$ is not a typical part of a modern inverse problem, but can be readily included (given the simplifying assumptions discussed in section 2) as a linear combination of temperature and salinity.

[21] Another constraint imposed on the solution is for the model state to vary smoothly. Grid-scale

noise is not acceptable. This prior information is supplied in a nondiagonal state covariance matrix. The diagonal elements of the matrix are based upon the expected variance of the model state, and the off-diagonal elements are nonzero for expected covariance between neighboring grid points. The expected covariance imposes a penalty for large second derivatives of the model fields (see *McIntosh and Veronis* [1993] and references therein for details on smoothness constraints). Here, we impose smoothing that corresponds to an e-folding distance of 4° in longitude and 750 meters in depth. Without constraining the solution to be smooth, model results would tend to satisfy observations by generating localized anomalies without changing the large-scale structure. The smoothness constraint is found to give an estimate of modern meridional transport consistent with those of previous investigators (to be shown in section 4.1).

[22] The mathematical treatment is identical for dynamical constraints and observations; both are linear equations which must be satisfied within some accuracy. Observations should not be fit exactly by the model because one does not wish to also fit the observational noise. As indicated by ϵ in the thermal wind equation, the dynamical balances are not perfect, either. By treating the model state, the noise in the observations, and the dynamical imbalances as the unknown variables, the inverse problem reduces to nothing more than solving a set of simultaneous linear equations. The Gauss-Markov method is used to solve this set of linear equations subject to our prior expectations of the solution characteristics involving the selected uncertainties and smoothness constraints; see *Wunsch* [1996] or *Tarantola* [1987] for details.

4. Inversions of Modern Hydrography and $\delta^{18}\text{O}$

[23] The null-hypothesis we seek to reject is that zonally averaged meridional transport at 30°S is the same during the LGM and modern periods. The alternate hypothesis is that there is some difference. To our knowledge, it has not been previously shown that a null-hypothesis involving the LGM circulation of mass can be statistically rejected, and we take this as the logical starting point. Note, however, that if the null-hypothesis can be rejected, it will still be necessary to ascertain what change is required, and what the climatic significance of such a change is.

[24] Five separate model inversions are performed: (1) An inversion of modern temperature and salinity which provides a standard against which paleo-inversions are compared. (2) An inversion of the Holocene $\delta^{18}\text{O}_{\text{calcite}}$ shows that these observations are consistent with the modern hydrography. (3) LGM $\delta^{18}\text{O}_{\text{calcite}}$ observations, taken alone, admit nearly perfect agreement with modern meridional transport. (4) Inversion 4 repeats 3, but uses idealized observations to investigate why $\delta^{18}\text{O}_{\text{calcite}}$ alone is not enough to reject the null-hypothesis. (5) Finally, LGM $\delta^{18}\text{O}_{\text{calcite}}$ are inverted along with assumed temperatures (the modern), and in this case, meridional transports different from the modern are required by the data.

4.1. Reference Inversion from Modern Hydrography

[25] Inversion 1 provides a reference circulation using modern observations of temperature and salinity from the HydroBase2 climatology [Curry, 2002]. Uncertainties are specified to be uniform with depth, $\pm 0.01^\circ\text{C}$ for temperature and ± 0.01 for salinity, although the actual uncertainties vary with depth. The zonal model resolution is the same as the HydroBase climatology, so no interpolation (beyond that done for HydroBase) is necessary. Our vertical grid subsamples the HydroBase climatology.

[26] Uncertainties in the total volume flux across 30°S are estimated from observations. Modern measurements show that the Bering Strait through-flow is 0.9 ± 1 Sv into the Arctic Ocean [Roach *et al.*, 1995]. Volume flux across 30°S also depends upon the Ekman transport, estimated to be 0.2 Sv southward from ECMWF ERA-40 wind reanalysis [Gibson *et al.*, 1997]. Note that the annual average Ekman flux is small, but the seasonal amplitude of Ekman transport is 5 Sv, highlighting the possibility that even moderate changes in the seasonal wind stress, perhaps due to the changing length of seasons, could cause circulations different from today. Neglecting the relatively small contributions from evaporation, precipitation, and runoff, the geostrophic transport across 30°S is set to -1.1 Sv (southward) with an uncertainty of 1 Sv.

[27] In total, there are 4212 observations of temperature and salinity, 2099 thermal wind constraints, and 1 mass conservation constraint, for a total of 6312 constraints. The model state, however, has 6346 elements and the problem is formally underdetermined. Examination of this underdetermined component, i.e., the null space,

shows that a depth-independent velocity can be added to any column so long as the other columns compensate to keep the total transport balanced. The reference-level velocity problem (parameter V_o in equation (3)) reappears in this way. Due to variations in the seafloor depth, depth-independent velocity can also affect the overturning circulation, as discussed more fully below.

[28] The temperature, salinity, and density estimated by the model inversion are shown in Figure 2. As expected, given the small specified uncertainties, temperature and salinity are almost identical to the HydroBase data set. In the interior, the isopycnals generally slope upward toward the east indicative of the subtropical gyre circulation. Furthermore, the African margin is denser than the South American side everywhere above 2000 meters depth.

[29] The modern velocity field has a magnitude of less than 3 cm/s everywhere (see Figure 3). The zonally integrated transport switches from northward to southward flow at 1200 meters, but the zero velocity line does not mark any water-mass boundaries, nor is it confined to the deep ocean, and it is difficult to zonally integrate the figure “by eye.” There is a net southward transport of 22 Sv below 1200 meters, and a nearly compensating 21 Sv of northward transport in the upper ocean, the remainder owing to inflow from the Arctic Ocean. Neglecting model error, the uncertainty of the implied maximum Atlantic overturning is ± 2 Sv, but this is a lower bound. Other investigators [e.g., Ganachaud and Wunsch, 2000; Talley, 2003] find overturning rates in the South Atlantic between 15–25 Sv with reported errors of 2–4 Sv. The uncertainty in the transport at each model level is small except at the surface level, because the grid layout does not permit calculation of the thermal wind relation there.

[30] One conspicuous feature of the South Atlantic hydrography is a core of NADW water properties along the western boundary. In Figure 3, a weak southward current at 2000–3000 meters depth is associated with the NADW core, but the velocity may be underestimated due to model resolution along the margin. Below 3000 meters depth, the signature of Antarctic Bottom Water (AABW) is seen in the northward velocities on the South Atlantic margin (45°W) and the eastern flank of the Walvis Ridge (5°E).

[31] The depth-independent velocity contributes 2 Sv of southward transport below 3000 meters. The external mode projects onto the overturning

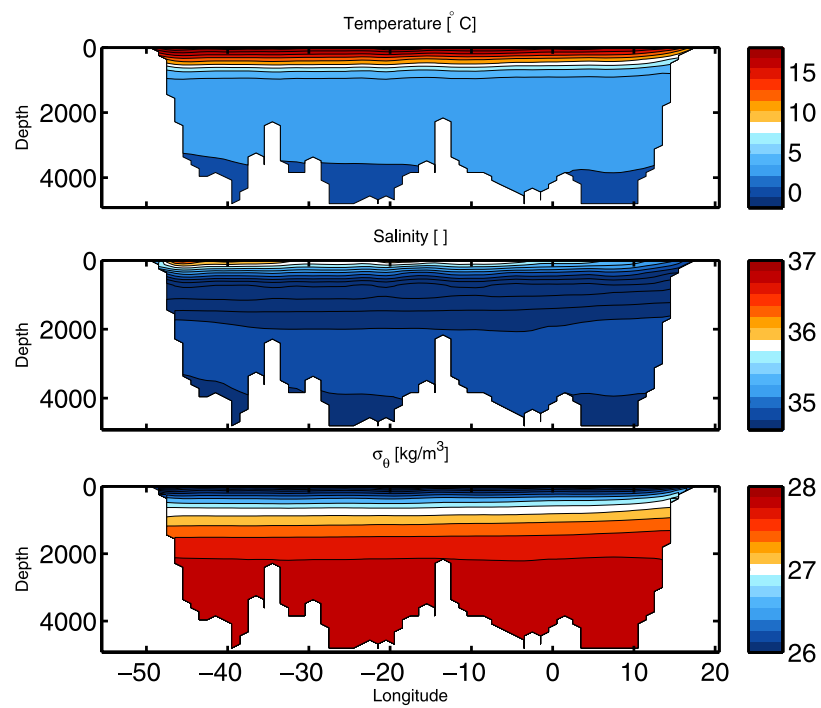


Figure 2. The (top) temperature, (middle) salinity, and (bottom) potential density (expressed as sigma theta) at 30°S from the modern reference inversion. Temperature and salinity strongly resemble the HydroBase2 climatology for the modern ocean.

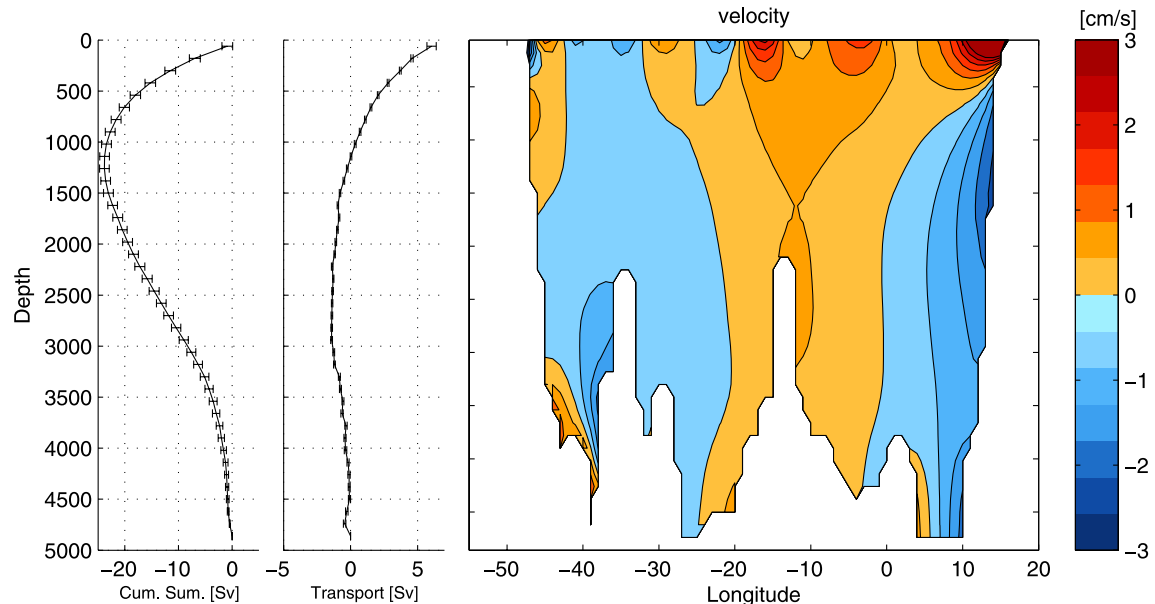


Figure 3. Inversion 1: The modern reference meridional velocity field at 30°S. (left) Cumulative sum of transport above the seafloor and its associated one-standard-deviation error bar in units of Sv. (middle) Zonally integrated transport for each model level and error bars. (right) Depth-longitude section of meridional velocity with a contour interval of 0.5 cm/s. Negative values represent southward transport.

circulation due to the topography. Above 3000 meters, there is a net transport of 1 Sv northward by the depth-independent velocity field, much smaller than the total overturning rate of 21 Sv.

4.2. Holocene $\delta^{18}\text{O}_{\text{calcite}}$ and the Modern Circulation

[32] Before proceeding with interpretation of the LGM $\delta^{18}\text{O}_{\text{calcite}}$ observations, it is important to first determine whether the Holocene $\delta^{18}\text{O}_{\text{calcite}}$ values are consistent with the modern circulation. For inversion 2, then, the model is constrained to reproduce the modern zonally integrated transport (from inversion 1) and Holocene $\delta^{18}\text{O}_{\text{calcite}}$ observations simultaneously. The acceptable size of the transport residuals are determined by the uncertainties associated with inversion 1, approximately ± 0.1 Sv for each vertical layer - a highly optimistic estimate which more readily permits rejection of the null-hypothesis. An uncertainty of $\pm 0.2\%$ is assigned to each $\delta^{18}\text{O}_{\text{calcite}}$ observation. These same uncertainties for transport and $\delta^{18}\text{O}_{\text{calcite}}$ will be used in all subsequent inversions.

[33] The assumed uncertainties in $\delta^{18}\text{O}_{\text{calcite}}$ used in this study are larger than those provided by [Lynch-Stieglitz *et al.*, 2006], because we wish to partially account for the uncertainties in the interpretation of the proxy as well as interlaboratory offsets. A more detailed investigation could assign uncertainties to each observation based on such factors as the completeness of the stratigraphy, variability in the $\delta^{18}\text{O}_{\text{calcite}}$ time series, potential for bioturbational influences, and how tightly the salinity- $\delta^{18}\text{O}_{\text{water}}$ relationship is constrained. Another important source of error results from collapsing the data onto the 30°S section. A more complete error estimate should downweight data that come from more distant locations.

[34] The model makes a prediction of each $\delta^{18}\text{O}_{\text{calcite}}$ observation using equation (1) and by linearly interpolating temperature and salinity onto the depth of the data point. Modern transports are found to be consistent with Holocene $\delta^{18}\text{O}_{\text{calcite}}$ values (see Figure 4). The $\delta^{18}\text{O}_{\text{calcite}}$ residuals between observations and model values have a negligible mean and a standard deviation of 0.21‰ on the eastern margin and 0.13‰ on the western margin, consistent with the assumed uncertainty of $\pm 0.2\%$. Transports are everywhere within one standard deviation of the modern except for a slightly larger discrepancy in the upper layer.

We thus conclude that the Holocene $\delta^{18}\text{O}_{\text{calcite}}$ is consistent with the modern circulation.

[35] As an additional test, temperature is specified to remain within 1°C of the modern values at each location for which $\delta^{18}\text{O}_{\text{calcite}}$ observations are available. Model temperatures are warmer by 0.6°C on the eastern margin, somewhat larger than expected by chance, but this is only one value out of six (standard deviation and mean for temperature, $\delta^{18}\text{O}_{\text{calcite}}$, and transport) so that the overall fit is a good one. It thus appears that the Holocene $\delta^{18}\text{O}_{\text{calcite}}$ is consistent with the modern overturning circulation and the modern temperature distribution.

4.3. Inversion of LGM $\delta^{18}\text{O}$ Alone

[36] Next, we wish to investigate whether the LGM $\delta^{18}\text{O}_{\text{calcite}}$ observations are consistent with the modern overturning circulation. A direct comparison between modern and LGM circulations is hampered by the difference in sea level. To distinguish sea level change from other effects, we first find the circulation that would result from the modern hydrography but the LGM bathymetry. Model sea level is lowered by removing the top grid level, and then shifting the modern temperature and salinity downward by 120 meters. Temperatures and salinities shifted into the seafloor are discarded. While it is unrealistic for the hydrography to have merely shifted downward without any other distortion, this at least provides a more consistent reference state to compare against the LGM circulation. In addition, the Bering Strait is now closed, and hence, there is no net throughflow across 30°S.

[37] Repeating inversion 1, but now with the LGM bathymetry and shifted temperature and salinity, yields a velocity structure (not shown) similar to the modern case, but with net northward transport of the upper ocean reduced from 22 Sv to 18 Sv. This change results from the removal of strong currents along the upper margins and continental shelf, while the change in cross-sectional area has only a minor effect. Note that more complete models which include the effects of tidal dissipation suggest that the exposure of the continental shelves, rather than leading to reduced circulation, could result in greater tidal mixing in the abyss [Egbert *et al.*, 2004] and increased meridional circulation rates.

[38] Having obtained a reference circulation from modern hydrography, an initial inversion of the

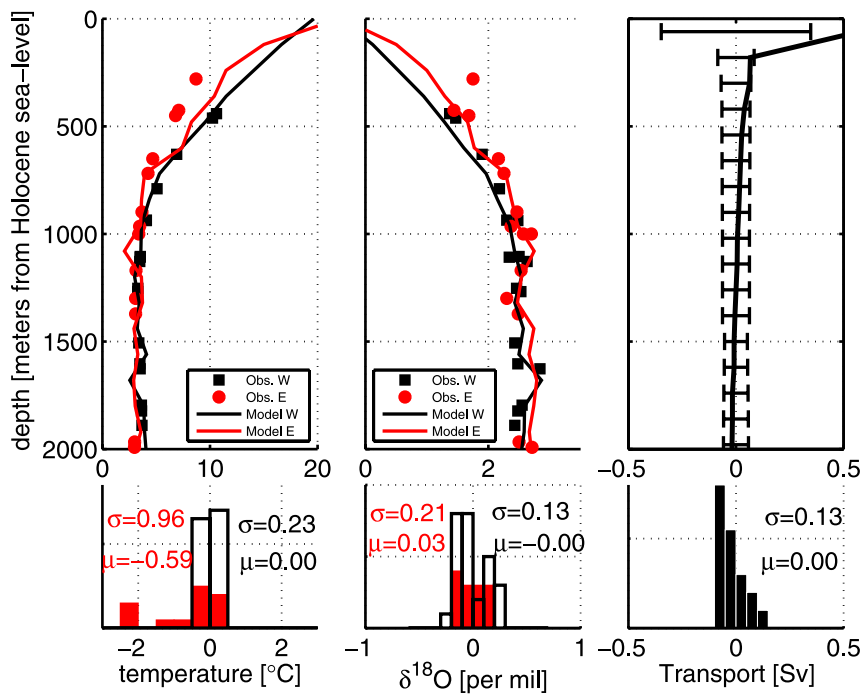


Figure 4. Inversion 2: Test of Holocene $\delta^{18}\text{O}_{\text{calcite}}$ observations against the modern reference circulation. (top left) Model temperature on the eastern margin (red line) and western margin (black line) compared to modern values of temperature (circles, squares) at the sites of $\delta^{18}\text{O}_{\text{calcite}}$ observations. (bottom left) Differences between modern and model temperature on the western margin (black histogram) and eastern margin (red histogram); σ and μ indicate the associated standard deviations and mean values. (top middle) Comparison of Holocene $\delta^{18}\text{O}_{\text{calcite}}$ measurements on the western margin (black squares) and eastern margin (red circles) with model values of $\delta^{18}\text{O}_{\text{calcite}}$ (black line and red line, respectively) as a function of depth. (bottom middle) Differences between observed and modeled $\delta^{18}\text{O}_{\text{calcite}}$ on the western margin (black histogram) and eastern margin (red histogram). (top right) Changes in the model transport relative to the modern reference circulation as a function of depth, and the error bar for the modern circulation. (bottom right) Histogram of differences in transport, and the standard deviation and mean of these differences. Note that the changes to the transport are one order of magnitude smaller than the overall transport (see Figure 3) and that the histogram includes residuals from below 2000 meters.

LGM $\delta^{18}\text{O}_{\text{calcite}}$ observations is now presented (inversion 3). The model is constrained to meet modern estimates of meridional transport and the LGM observations of $\delta^{18}\text{O}_{\text{calcite}}$ within their estimated uncertainties. For the $\delta^{18}\text{O}_{\text{calcite}}$ observations to permit rejection of the null-hypothesis, the model should be incapable of simultaneously meeting the meridional transport and $\delta^{18}\text{O}_{\text{calcite}}$ requirements, and large residuals would be expected between the model solution and the imposed observational and transport requirements. However, the model is able to meet both the $\delta^{18}\text{O}_{\text{calcite}}$ observations and modern transport requirements within their specified uncertainties (Figure 5). The standard deviation of the difference between the Glacial and modern circulations is 0.05 Sv, below the uncertainty in the modern circulation (0.1 Sv). The misfit between $\delta^{18}\text{O}_{\text{calcite}}$ data and the model has a standard deviation of 0.19‰, near the expected uncertainty of 0.2‰.

[39] The vertical resolution of the observations is important, as seen by the vertical profile of the modeled $\delta^{18}\text{O}_{\text{calcite}}$. Even with an imposed smoothness criterion on the model fields, the $\delta^{18}\text{O}_{\text{calcite}}$ profile has excursions of 0.5‰ at depths without any data. From these results, it seems possible that the vertical resolution of the data is inadequate, or the noise in the observations is too large to permit rejection of the null-hypothesis. Another possibility is that the model's imposed changes in $\delta^{18}\text{O}_{\text{calcite}}$ are unrealistic. To address these issues, we propose an idealized extension to inversion 3 next.

4.4. Inversion of Idealized LGM $\delta^{18}\text{O}$

[40] Inversion 4 proceeds with an idealized scenario for the $\delta^{18}\text{O}_{\text{calcite}}$ observations. An underlying smooth function of $\delta^{18}\text{O}_{\text{calcite}}$ with depth is found by fitting the data to a third-order polynomial, and this smooth and fully resolved function is used as

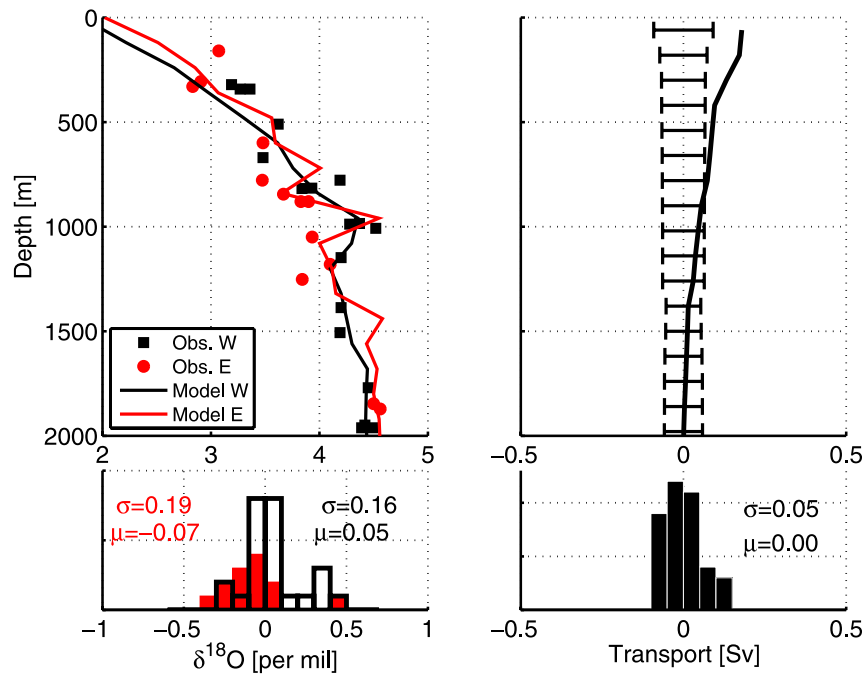


Figure 5. Inversion 3: Test of LGM $\delta^{18}\text{O}_{\text{calcite}}$ measurements against the modern reference circulation. The format follows the middle and right panels from Figure 4.

the new “data” in inversion 4 (Figure 6, top left panel, open circles and squares). The standard deviation of the misfit between the observations and the polynomial is 0.14‰.

[41] Even in this case, the model is able to simultaneously meet the $\delta^{18}\text{O}_{\text{calcite}}$ observations and modern transport requirements within their specified uncertainties (see Figure 6, bottom panels). The standard deviation of the difference between the Glacial and modern circulations is 0.08 Sv, below the uncertainty in the modern circulation (0.1 Sv). The smoothed $\delta^{18}\text{O}_{\text{calcite}}$ data is satisfied to within $\pm 0.02\text{‰}$, a nearly perfect fit. It is now possible to attribute the 0.19‰ error of inversion 3 primarily to the scatter in the data. Inversion 4 shows that neither the vertical resolution nor the observational noise leads to the failure to reject the null-hypothesis; rather, there is another shortcoming to be discussed next.

[42] To fit both the modern circulation and LGM $\delta^{18}\text{O}_{\text{calcite}}$, the model finds a loophole by which to disassociate $\delta^{18}\text{O}_{\text{calcite}}$ and density. There exists an infinite number of combinations of temperature and salinity that give the same cross-basin $\delta^{18}\text{O}_{\text{calcite}}$ gradient, but each combination has a different cross-basin density gradient, the crucial quantity

for the overturning circulation. The intersecting $\Delta(\delta^{18}\text{O}_{\text{calcite}})$ and $\Delta\rho$ iso-lines of Figure 7 illustrate this point. Density is more sensitive to changes in salinity, relative to temperature, than is $\delta^{18}\text{O}_{\text{calcite}}$, thus explaining the nonparallel lines. Making the lines of constant density and $\delta^{18}\text{O}_{\text{calcite}}$ nearly parallel would eliminate the loophole, but would require a $\delta^{18}\text{O}_{\text{calcite}}\text{-S}$ coefficient of approximately $a = 1.3\text{‰}$, more than twice as large as the modern South Atlantic estimate. Given only observations of $\delta^{18}\text{O}_{\text{calcite}}$, therefore, nearly any cross-basin density difference is possible, so long as temperature and salinity compensate each other.

[43] The cross-basin differences of temperature and salinity for inversions 1 and 4 are also plotted in Figure 7. In the modern hydrography, both density and $\delta^{18}\text{O}_{\text{calcite}}$ are greater on the African margin. For the LGM, inversion 4 indicates that the LGM temperature is greater on the African margin, in contrast to the Holocene situation. However, inversion 4 also introduces greater salinities on the African margin relative to South America, and the cross-basin density difference is nearly unchanged. The shaded areas of Figure 7 indicate regions where the cross-basin density and $\delta^{18}\text{O}_{\text{calcite}}$ differences can have the opposite sign. Inversion 4 shifts temperature and salinity for the LGM such

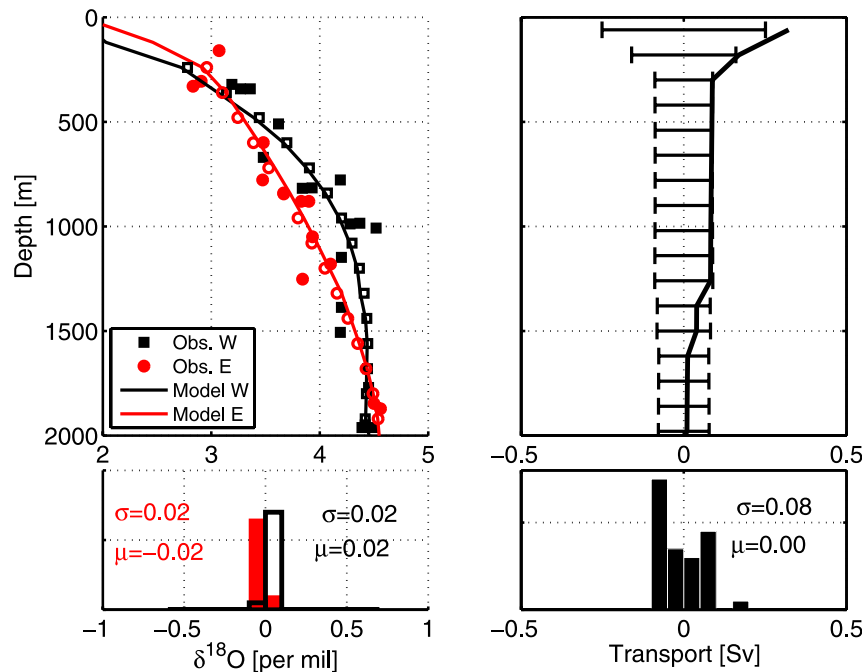


Figure 6. Inversion 4: Test of LGM $\delta^{18}\text{O}_{\text{calcite}}$ measurements against the modern reference circulation with smoothed and interpolated data. In the same format as Figure 5, except the inversion uses a polynomial fit (open symbols) derived from the actual observations (closed symbols). The bottom left panel shows histograms of the residuals between the polynomial-fit data (open symbols) and the model estimate (solid lines).

that this disassociation between density and $\delta^{18}\text{O}_{\text{calcite}}$ is exploited.

[44] Before accepting the consistency of the modern overturning circulation and LGM $\delta^{18}\text{O}_{\text{calcite}}$, it is necessary to consider whether the model temperature and salinity changes are reasonable. The top panels of Figure 8 show LGM temperature and salinity profiles relative to the modern hydrography. Between 500 and 1500 meters depth, the $\delta^{18}\text{O}_{\text{calcite}}$ observations require an LGM cross-basin temperature difference of 3°C , and cross-basin salinity differences of 0.7, while modern cross-basin differences at mid-depths are much smaller ($<1^{\circ}\text{C}$ and <0.2 for salinity). Although temperature and salinity along the African margin are different than anything observed in the modern South Atlantic, they do resemble the temperature and salinity of the modern subtropical North Atlantic Ocean.

[45] The water-mass properties of the modern and LGM cases are pictured on a temperature-salinity diagram (Figure 8, bottom panel). The modern T-S curves show the distinct characteristics of South Atlantic Central Water (SACW), Antarctic Intermediate Water (AAIW), NADW, and AABW. The LGM T-S curve for the South American margin

differs from the African margin at mid-depths, and these differences could be explained by changes in the characteristics and quantity of AAIW. While the South American margin has AAIW at lower temperatures and salinities than modern AAIW, the African margin has almost no AAIW at all. Although the LGM T-S curves look different than their modern counterparts at 30°S , it is possible to find modern T-S curves from other parts of the ocean which look similar to the LGM examples. In summary, even though water-mass constraints have not been placed on the inversion here, it appears that no obvious violations of water-mass properties have occurred in inversion 4. A complete plausibility analysis of the shift in water-mass properties, however, would require a more complete dynamical model.

[46] Ideally, a temperature estimate would be available for each Holocene and LGM observation of $\delta^{18}\text{O}_{\text{calcite}}$. Currently, we only know of one LGM Mg/Ca temperature estimate at a mid-depth site on the Brazil margin, indicating approximately stable temperatures through the glacial and Holocene [Bill Curry, personal communication]. In addition, South Atlantic sea surface temperature estimates for the LGM indicate values within 1°C of the

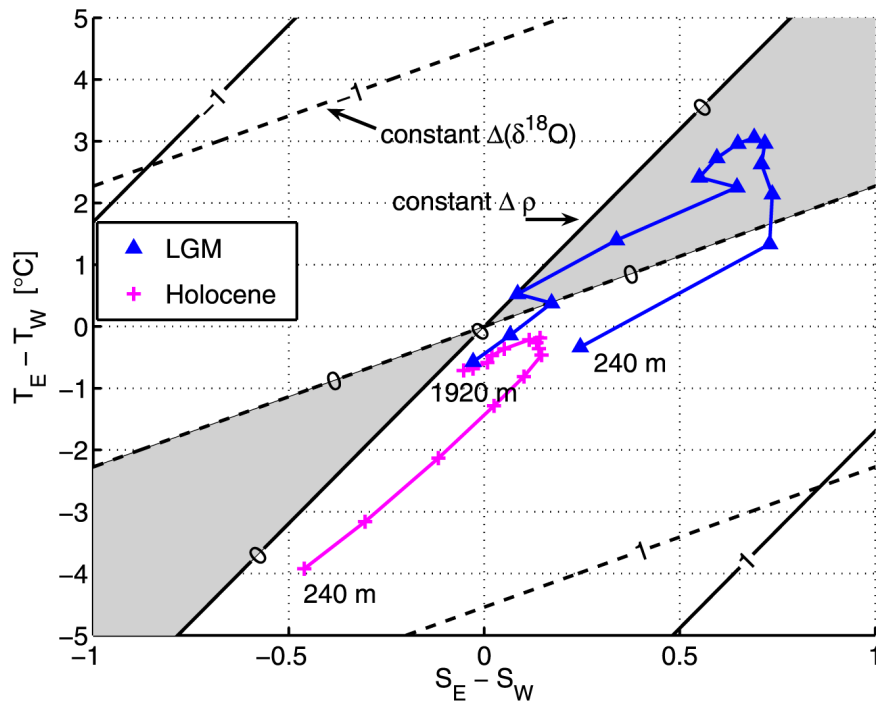


Figure 7. Scatterplot of the cross-basin differences in temperature and salinity in the upper 2000 meters. The x axis is the difference between salinity on the eastern margin and the western margin; east-west temperature differences are marked on the y axis. Solid lines indicate constant density, while dashed lines indicate constant $\delta^{18}\text{O}_{\text{calcite}}$. Model $\Delta T - \Delta S$ pairs from inversion 1 are marked with magenta pluses, and model pairs from inversion 4 are shown with blue triangles. The shaded region indicates where the cross-basin density and $\delta^{18}\text{O}_{\text{calcite}}$ are of opposite sign. For example, the blue triangles in the shaded region are associated with $\delta^{18}\text{O}_{\text{calcite}}$ values that are larger on the South American margin, while at the corresponding vertical level, density is larger on the African margin. A constant density equation is assumed, equivalent to the linearization at 1000 meter depth.

modern [Mix *et al.*, 1999]. Thus it is plausible that temperatures near 30°S have remained nearly stable since the last glacial, and therefore it is useful to explore the interpretation of the $\delta^{18}\text{O}_{\text{calcite}}$ when temperature changes are restricted to a more narrow range. Note that while we choose to explore additional temperature constraints, pore water constraints on salinity could also serve to close the loophole by which density and $\delta^{18}\text{O}_{\text{calcite}}$ vary independently of one another.

4.5. LGM $\delta^{18}\text{O}$ and Temperature

[47] Inversion 5 constrains the model to have modern transports, modern temperatures, and the LGM $\delta^{18}\text{O}_{\text{calcite}}$. Unlike inversions 3 and 4, this inversion produces large residuals in both temperature and $\delta^{18}\text{O}_{\text{calcite}}$ (see Figure 9). The residuals indicate a systematic shift of the entire western margin toward lower model temperature and lower model $\delta^{18}\text{O}_{\text{calcite}}$ values than indicated in the data, with an opposite shift on the eastern margin. The residuals act to maintain the modern cross-basin density difference.

[48] The model residuals are highly significant. The eastern $\delta^{18}\text{O}_{\text{calcite}}$ residuals have a mean value of $-0.17\text{\textperthousand}$. The probability of this mean value occurring by chance, assuming a normally distributed population, is $p = 0.002$. In addition, the mean value of western $\delta^{18}\text{O}_{\text{calcite}}$ residuals also permits rejection of the null-hypothesis of no change in meridional circulation, but with a lower 95% confidence level ($p = 0.04$). Temperature and transport residuals are also large relative to their uncertainties, and in this case, some change away from the modern meridional circulation appears necessary.

[49] It is useful to check whether a looser constraint on meridional transports would also permit rejection of the null hypothesis. Another inversion is performed wherein the model is required to transport 18 Sv northward in the upper 1500 meters but the exact vertical profile is left unspecified. In this case, mean changes in $\delta^{18}\text{O}_{\text{calcite}}$ are about one-third smaller than for inversion 5, but these are still significant and oriented so as to reduce the cross-basin density gradient. Temperature and

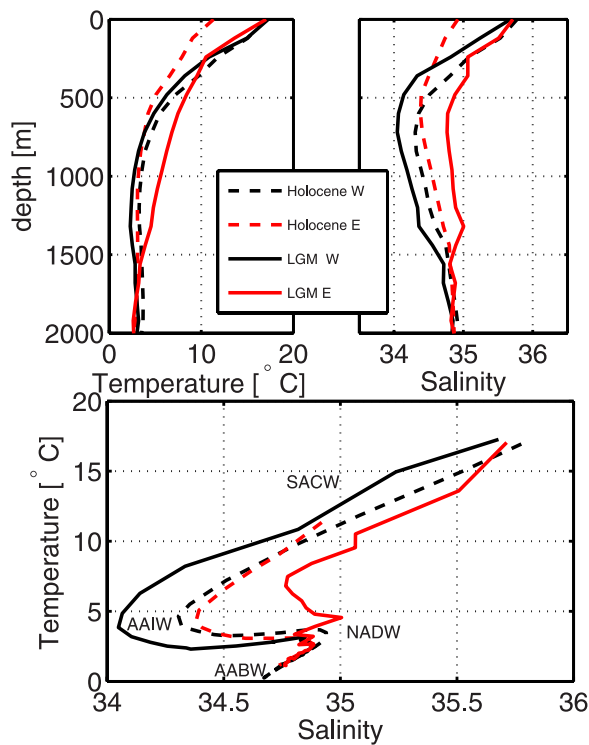


Figure 8. (top left) Temperature profile with depth from inversion 1 on the South American margin (Holocene W) and the African margin (Holocene E) compared to inversion 4 for the South American margin (LGM W) and the African margin (LGM E). (top right) In the same format as the top left, but for salinity. (bottom) A T-S diagram from the same temperature and salinity profiles, but including the entire water column. Modern South Atlantic Central Water (SACW), Antarctic Intermediate Water (AAIW), North Atlantic Deep Water (NADW), and Antarctic Bottom Water (AABW) have been marked on the diagram for reference.

transport residuals are nearly the same as in inversion 5. Both this more loosely constrained inversion and inversion 5 indicate that a change from the modern circulation is necessary.

[50] A final inversion is performed to find the transport most consistent with modern temperatures and LGM $\delta^{18}\text{O}_{\text{calcite}}$. In this case, the model actually reverses the modern flow field, producing 5 Sv of transport to the south in the upper 1000 m and a weak northward return flow at depth. This result owes to the reversal of the LGM cross-basin $\delta^{18}\text{O}_{\text{calcite}}$ gradient relative the modern. Given the strong assumptions which have been made regarding temperature, salinity, and density, however, the result of this inversion should not be considered an actual estimate of past transport.

[51] In the foregoing inversions the Ekman transport was fixed to 0.2 ± 1 Sv, consistent with

modern observations. But if larger Ekman transports were imposed, as may be the case for the LGM, model residuals would not change as long as the Ekman transport was compensated by a depth-independent return flow in all layers. In other words, such a shift in the overturning circulation would be undetectable given the observations and dynamical model used here. In general, winds help set up the stratification of the ocean, and thus there is some connection between the wind field and the velocity shear of the ocean, but this link is not explicitly included in our model. Inclusion of dynamical constraints between the wind and overturning circulation will necessarily require a more complete ocean model [e.g., Jayne and Marotzke, 2001].

[52] Hirschi and Lynch-Stieglitz [2006] explore the estimation of meridional circulation rates from ocean margin densities using a forward model and find that, even using a small number of density observations, it is possible to reconstruct changes in past circulation. Our results indicate that it could be more difficult to constrain the circulation because of possible systematic shifts in the relationship between $\delta^{18}\text{O}_{\text{calcite}}$ and density, as well as changes in Ekman transport. The systematic errors explored by Hirschi and Lynch-Stieglitz involve changing from an Atlantic to Pacific type relationship between $\delta^{18}\text{O}_{\text{calcite}}$ and density, but as discussed, it seems difficult to rule out even larger systematic errors when changing from a modern to LGM climate.

5. Summary and Conclusions

[53] Following the work of Legrand and Wunsch [1995], a path is traced toward testing past circulation rates through combining dynamics and observations. The dynamics include geostrophic balance, hydrostatic balance, and conservation of mass. Observations come from a new compilation of $\delta^{18}\text{O}_{\text{calcite}}$ measurements from the margins of the South Atlantic. Two explanations were shown to account for the $\delta^{18}\text{O}_{\text{calcite}}$ observations: one a change in water-mass properties (inversion 4) and another a change in the mass circulation (inversion 5). For the model inversion to require a meridional circulation different from the modern, a number of assumptions were necessary: a relationship between $\delta^{18}\text{O}_{\text{water}}$ and salinity fixed at $0.5\Delta\text{‰}/\Delta S$, offset parameters of the $\delta^{18}\text{O}_{\text{water}}$ -salinity relationship with no spatial variations, and LGM temperatures similar to the modern temperatures.

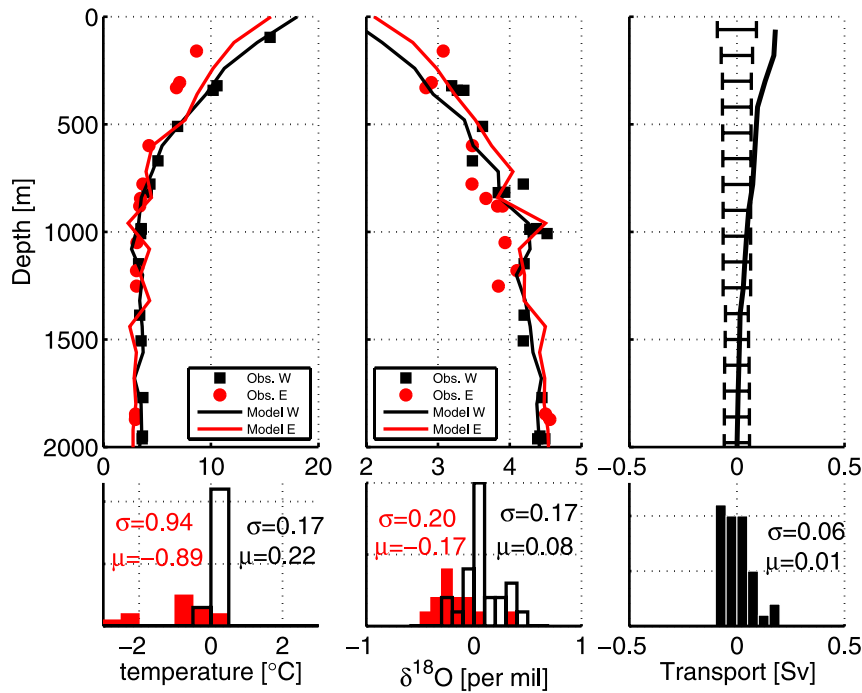


Figure 9. Inversion 5: Test of LGM $\delta^{18}\text{O}_{\text{calcite}}$ measurements and modern temperatures against the modern reference circulation. Figure format follows that of Figure 4.

[54] There is a need for further observations to distinguish between the above two scenarios. Ideally one would have a transect of $\delta^{18}\text{O}_{\text{calcite}}$ observations along a single latitude band from South America to Africa. Each $\delta^{18}\text{O}_{\text{calcite}}$ observation would be complemented by a temperature estimate, possibly from Mg/Ca ratios. Furthermore, pore-water from sediment cores along the South American and African margins would constrain past values of salinity and $\delta^{18}\text{O}_{\text{water}}$. Strictly speaking, in this case, the $\delta^{18}\text{O}_{\text{calcite}}$ would not be necessary as temperature and salinity could be independently deduced, but this would permit checks of consistency and more accurate constraints. It seems that $\delta^{18}\text{O}_{\text{calcite}}$ is more easily measured than pore-water profiles and would be more amenable to providing dense spatial coverage.

[55] There are also a number of other lines of information which could be drawn upon. $\delta^{18}\text{O}_{\text{water}}$ also functions as a conservative tracer which could aid in distinguishing water mass properties, as could other tracers such as $\delta^{13}\text{C}$. The distribution of these quantities is taken into account in the interpretation of the data by *Lynch-Stieglitz et al.* [2006]. Formally integrating additional tracer information into the model could most directly be achieved by extending the model domain to three dimensions and explicitly including tracer transport

in the model dynamics. This would tend to generate more distinct mixing ratios of temperature, salinity, and $\delta^{18}\text{O}_{\text{water}}$, as observed for the modern ocean. Alternatively, water mass properties could be identified with a source region and the present zonal model constrained to generate a flow field having transport from those regions. Given difficulties in inferring rates of transport from tracers suggests using nonnegative least squares, wherein the direction of flow could be specified, even if the speed is not. It is thus possible that extending the model used here to include more dynamical and observational constraints would permit better determination of past circulation. But it should also be kept in mind that the inclusion of additional processes, if not adequately constrained by paleo-observations, may increase the complexity of the model without increasing its skill, and serve only to make the results more difficult to interpret.

[56] While the ambiguities involved in interpreting any one proxy render its climatic significance uncertain, taking multiple proxies together should make it possible to determine the relevant features of the past ocean circulation. Eventually, one hopes for a model platform in which a global paleo-observational network could be integrated. As the paleoceanographic database grows and it becomes better integrated into a modeling frame-

work, the combination of data and models should increasingly bear a fruitful understanding of the past ocean circulation.

Acknowledgments

[57] The authors wish to thank Jean Lynch-Stieglitz, Bill Curry, Delia Oppo, Ulysses Ninneman, Christopher Charles, and Jenna Munson for making their data set available for analysis. Bill Curry, Delia Oppo, Jerry McManus, Jean Lynch-Stieglitz, Carl Wunsch, Olivier Marchal, Zan Stine, David Lund, and an anonymous reviewer provided useful guidance. P.H. was funded by the NOAA postdoctoral program in climate and global change, and G.G. was partially funded by NSF paleoclimate program ATM-0502482.

References

- Adkins, J., K. McIntyre, and D. Schrag (2002), The salinity, temperature, and $\delta^{18}\text{O}$ of the glacial deep ocean, *Science*, 298, 1724–1725.
- Boyle, E. (1990), Quaternary deepwater paleoceanography, *Science*, 249, 863–870.
- Curry, R. G. (2002), Hydrobase2: A database of hydrographic profiles and tools for climatological analysis, Woods Hole Oceanogr. Inst., Woods Hole, Mass. (Available at <http://www.whoi.edu/science/PO/hydrobase>)
- Curry, W. B., and D. W. Oppo (2005), Glacial water mass geometry and the distribution of $\delta^{13}\text{C}$ of σCO_2 in the western Atlantic Ocean, *Paleoceanography*, 20, PA1017, doi:10.1029/2004PA001021.
- Egbert, G. D., R. D. Ray, and B. G. Bills (2004), Numerical modeling of the global semidiurnal tide in the present day and in the last glacial maximum, *J. Geophys. Res.*, 109, C03003, doi:10.1029/2003JC001973.
- Ganachaud, A., and C. Wunsch (2000), Improved estimates of global ocean circulation, heat transport and mixing from hydrographic data, *Nature*, 408(6811), 453–457.
- Gibson, J., S. Kallberg, S. Uppala, A. Nomura, A. Hernandez, and E. Serrano (1997), ECMWF reanalysis project report series no.1 technical report 1, technical report, Eur. Cent. for Medium-Range Weather Forecasts, Reading, U. K.
- Hirschi, J. J.-M., and J. Lynch-Stieglitz (2006), Ocean margin densities and paleoestimates of the Atlantic meridional overturning circulation: A model study, *Geochem. Geophys. Geosyst.*, 7, Q10N04, doi:10.1029/2006GC001301.
- Huybers, P., G. Gebbie, and O. Marchal (2006), Can paleoceanographic tracers constrain meridional circulation rates?, *J. Phys. Oceanogr.*, in press.
- Jayne, S. R., and J. Marotzke (2001), The dynamics of ocean heat transport variability, *Rev. Geophys.*, 39(3), 385–411.
- Kucera, M., A. Rosell-Mele, R. Schneider, C. Waelbroeck, and M. Weinelt (2006), Multiproxy approach for the reconstruction of the glacial ocean surface (MARGO), *Quat. Sci. Rev.*, 24.
- Legrand, P., and C. Wunsch (1995), Constraints from paleotracer data on the North Atlantic circulation during the last glacial maximum, *Paleoceanography*, 10, 1011–1045.
- LeGrande, A., G. Schmidt, D. Shindell, C. Field, R. Miller, D. Koch, G. Faluvegi, and G. Hoffmann (2006), Consistent simulations of multiple proxy responses to an abrupt climate change event, *Proc. Natl. Acad. Sci. U. S. A.*, 103, 837–842, doi:10.1073/pnas.0510095103.
- Lynch-Stieglitz, J. (2001), Using ocean margin density to constrain ocean circulation and surface wind strength in the past, *Geochem. Geophys. Geosyst.*, 2(12), doi:10.1029/2001GC000208.
- Lynch-Stieglitz, J., W. B. Curry, and N. Slowey (1999), A geostrophic transport estimate for the Florida Current from the oxygen isotope composition of benthic foraminifera, *Paleoceanography*, 14(3), 360–373.
- Lynch-Stieglitz, J., W. B. Curry, D. W. Oppo, U. S. Ninneman, C. D. Charles, and J. Munson (2006), Meridional overturning circulation in the South Atlantic at the last glacial maximum, *Geochem. Geophys. Geosyst.*, 7, Q10N03, doi:10.1029/2005GC001226.
- Marotzke, J., R. Giering, K. Q. Zhang, D. Stammer, C. Hill, and T. Lee (1999), Construction of the adjoint MIT ocean general circulation model and application to Atlantic heat transport sensitivity, *J. Geophys. Res.*, 104, 529–547.
- McIntosh, P. C., and G. Veronis (1993), Solving underdetermined tracer inverse problems by spatial smoothing and cross validation, *J. Phys. Oceanogr.*, 23(4), 716–730.
- McManus, J. F., R. Francois, J.-M. Gherardi, L. D. Keigwin, and S. Brown-Leger (2004), Collapse and rapid resumption of Atlantic meridional circulation linked to deglacial climate changes, *Nature*, 428, 834–837.
- Mix, A., A. E. Morey, N. G. Pisias, and S. W. Hostetler (1999), Foraminiferal faunal estimates of paleotemperature: Circumventing the no-analog problem yields cool ice age tropics, *Paleoceanography*, 14(3), 350–359.
- Roach, A. T., K. Aagaard, C. H. Pease, S. A. Salo, T. Weingartner, V. Pavlov, and M. Kulakov (1995), Direct measurements of transport and water properties through the Bering Strait, *J. Geophys. Res.*, 100(C9), 18,443–18,457.
- Robinson, L., J. Adkins, L. Keigwin, J. Suthon, D. Fernandez, S. Wang, and D. Scheirer (2005), Radiocarbon variability in the western North Atlantic during the last deglaciation, *Science*, 310(5735), 1469–1473.
- Rohling, E., and G. Bigg (1998), Paleosalinity and $\delta^{18}\text{O}$: A critical assessment, *J. Geophys. Res.*, 103(C1), 1307–1318.
- Schmidt, G. (1998), Oxygen-18 variations in a global ocean model, *Geophys. Res. Lett.*, 25, 1201–1204.
- Schmidt, G., G. Bigg, and E. Rohling (1999), Global seawater oxygen-18 database, NASA Goddard Inst. for Space Stud. New York. (Available at <http://data.giss.nasa.gov/o18data/>)
- Talley, L. D. (2003), Data-based meridional overturning streamfunctions for the global ocean, *J. Clim.*, 16, 3213–3226.
- Tarantola, A. (1987), Inverse Problem Theory: Methods for Data Fitting and Model Parameter Estimation, 232 pp., Elsevier, New York.
- Thompson, W. G., and S. L. Goldstein (2005), Open-system coral ages reveal persistent suborbital sea-level cycles, *Science*, 308, 401–404.
- Toggweiler, J., and B. Samuels (1995), Effect of sea ice on the salinity of antarctic bottom waters, *J. Phys. Oceanogr.*, 25, 1980–1997.
- Winguth, A., D. Archer, E. Maier-Reimer, and U. Mikolajewicz (2000), Paleonutrient data analysis of the glacial Atlantic using an adjoint ocean general circulation model, in *Inverse Methods in Global Biogeochemical Cycles*, *Geophys. Monogr. Ser.*, vol. 114, edited by P. Kasibhatla et al., pp. 171–183, AGU, Washington, D. C.
- Wunsch, C. (1978), The general circulation of the North Atlantic west of 50°W determined from inverse methods, *Rev. Geophys.*, 16, 583–620.
- Wunsch, C. (1996), The Ocean Circulation Inverse Problem, 437 pp., Cambridge Univ. Press, New York.